HHS Public Access

Author manuscript

Magn Reson Med. Author manuscript; available in PMC 2019 October 01.

Published in final edited form as:

Magn Reson Med. 2018 October ; 80(4): 1289–1297. doi:10.1002/mrm.27121.

Unveiling a Hidden ^{31}P Signal Co-resonating with Extracellular Inorganic Phosphate by Outer-Volume-Suppression and Localized ^{31}P MRS at 7T

Jimin Ren[a,b,1], **Ty Shang**[c], **A. Dean Sherry**[a,b,d], and **Craig R. Malloy**[a,b,e,f]

[a]Advanced Imaging Research Center, University of Texas Southwestern Medical Center, Dallas, TX 75390.

[b]Department of Radiology, University of Texas Southwestern Medical Center, Dallas, TX 75390.

[c]Department of Neurology and Neurotherapeutics, University of Texas Southwestern Medical Center, Dallas, TX 75390.

[d]Department of Chemistry, University of Texas at Dallas, Richardson, TX 75080.

[e]Department of Internal Medicine, University of Texas Southwestern Medical Center, Dallas, TX 75390.

[f]VA North Texas Health Care System, Dallas, TX 75216.

Abstract

Purpose—The study was undertaken to demonstrate that there are more than one component in the extracellular inorganic phosphate ^{31}P signal (Pi^{ex}) acquired from human head using non-localized ^{31}P MRS.

Methods—Outer-volume-suppression (OVS) saturation and 1D/2D ^{31}P chemical shift imaging (CSI) were utilized to reveal the presence of an additional component in the Pi^{ex} signal.

Results—67% of the head extracellular Pi signal was attenuated upon OVS saturation of the peripheral meningeal tissues, likely reflecting elimination of the Pi signal in the meningeal fluids (the blood and CSF). Localized 1D/2D CSI data provided further support for this assignment. Upon correction for the meningeal contribution, the extracellular Pi concentration was 0.51 ± 0.07 mM, while the intracellular Pi was 0.85 ± 0.10 mM. The extracellular pH was measured as 7.32 ± 0.04 when using OVS, as compared to 7.39 ± 0.03 when measured without OVS (N = 7 subjects).

Conclusions—The extracellular Pi signal acquired from the human head using non-localized ^{31}P MRS contains a significant component likely contributed by peripheral blood and CSF in meninges that must be removed in order to use this signal as an endogenous probe for measuring extracellular pH and other properties in the brain.

[1]To whom correspondence should be addressed: Jimin Ren, 5323 Harry Hines Blvd, NE4.2, Dallas, Texas 75390-8568, USA, (214) 645-2722 Jimin.Ren@utsouthwestern.edu.

Keywords

brain; ^{31}P MRS; inorganic phosphate; pH; blood; CSF

INTRODUCTION

Several recent high field ^{31}P MRS studies in brain have detected two distinct inorganic phosphate (Pi) signals and assigned those to intra- and extracellular P_i (1–4). This observation holds great promise not only because it allows more reliable measurement of ATP energy consumption using the identified intracellular Pi signal (Pi^{in}) rather than a mixed signal (1–4), which is undistinguishable at lower field, but also because of the potential value of the extracellular Pi signal (Pi^{ex}) as an endogenous probe of the extracellular space (ECS). Such measurements in humans have been challenging technically but are critical for understanding normal brain processes as well as the pathophysiology of a variety of brain conditions and diseases such as tumors and traumatic brain injury (TBI) (5–14).

A question arises, however, as to whether the extracellular Pi signal observed by the conventional pulse-and-acquire (PA) ^{31}P MRS solely reflects Pi in the interstitial fluid (ISF) that bathes the neurons and glial cells. The possibility of presence of a P_i^{ex} component in addition to the ISF contribution is raised because the P_i^{ex}/P_i^{in} ratio obtained from quantitative ^{31}P MRS data (1) predicts an 40% higher P_i concentration than the documented value (0.5 – 1.0 mM) for the ISF (15), given the assumption of a normal ECS volume fraction of 20% (16, 17). A likely source for the unaccountable Pi^{ex} component could be the peripheral meningeal tissue, a layered structure under the skull enclosing the brain soft tissue, which is filled with Pi-containing fluids including cerebrospinal fluid (CSF) in the subarachnoid space and superficial venous blood flowing in the large sagittal and transverse sinuses.

Thus, the aim of the present work is 1) to evaluate whether a meningeal P_i component contributes to the P_i^{ex} signal acquired using a non-localized pulse sequence, and 2) to evaluate whether such a meningeal P_i component alters the measurement of extracellular pH. Given the peripheral location of the meninges relative to the parenchymal tissue of interest, we used an outer-volume-suppression (OVS) method to reduce contributions from potential meningeal components to the P_i^{ex} signal. Finally, localized 1D and 2D ^{31}P CSI methods were used to validate the OVS observations because of their capacity to differentiate meningeal from parenchymal tissues.

METHODS

Human Subjects

The protocol was approved by the Institutional Review Board of the University of Texas Southwestern Medical Center. Prior to the MRSI study, informed written consent was obtained from all participants. Eleven subjects (7 males and 4 females), aged 41.1 ± 13.8 yr, BMI 25.4 ± 2.6, resting heart rate 67.7 ± 10.9, and peripheral capillary oxygen saturation

(SpO2) 97.3 ± 2.1%, participated in the study. All subjects were in good general health with no history of peripheral vascular, systemic, myopathic, cancer, psychiatric or neurodegenerative diseases. Heart rate and blood oxygen saturation levels were monitored during the scan. The study was well-tolerated by all subjects.

MRS Protocol

All subjects were positioned head-first and supine in the MRI scanner (7T Achieva, Philips Healthcare, Best, The Netherlands), with the back of the head positioned on the center of the detection RF surface coil (Philips Healthcare, Best, The Netherlands). The coil was a half-cylinder-shaped, double-tuned $^{1}H/^{31}P$ quadrature TR coil consisting of two tilted, partially overlapping 10 cm loops. Axial, coronal, and sagittal T2-weighted turbo spin echo multi-slice images were acquired for ^{1}H shimming and ^{31}P MR MRS slice planning. Typical imaging parameters included field-of-view 180 × 180 mm^2 (FOV), repetition time (TR) 2.5 s, echo time (TE) 80 ms, turbo factor 15, in-plane spatial resolution 0.6 × 0.7 mm^2, slice thickness 8 mm, gap 2 mm, number of acquisitions (NA) one, and acquisition time 2.1 min. Second order ^{1}H-based automatic volume shimming was applied prior to ^{31}P spectral acquisitions.

Quantitative non-localized ^{31}P MR spectra were acquired as described previously (Ren et al (1)) using TR = 30 sec, number of acquisition (NA) 16, flip angle 55^{o}, sampling points 4096, spectral width 4 kHz, and a block-shaped excitation pulse with B_1 = 59 μT and pulse width 0.22 μs. The dead-time (DT, a delay following readout pulse and prior to data sampling) was set to 0.50 ms to filter out major broad baseline signals from the membrane phospholipids and the bones of the skull. For outer-volume-suppression (OVS), four ^{31}P saturation slabs with varying orientation were placed over the posterior meningeal and skull/scalp tissues, as guided by the T2w images. The saturation slabs were generated by a time and magnitude-modulated sine-shaped pulse with nominal B_{1max} 46 μT, duration 1.8 ms, and inter-pulse delay 2 ms, and applied immediately prior to the excitation pulse. Cares were taken to minimize potential spillover effect by placing the OVS slabs' inner edge close to the meninges-brain boundary to avoid large partial volume effect from over subscription of the inner brain tissues. A soft cushion pad (~ 3 cm thick) was placed under the neck to keep neck muscle away from the sensitive region of the coil and thus to avoid potential muscle contamination. The non-localized ^{31}P MRS data were acquired for seven subjects with OVS saturation on and off under otherwise identical acquisition conditions. The scan time was 16 mins for each measurement.

1D multi-slice MR spectra were acquired with slices arrayed in head-feet (HF) and anterior-posterior (AP) directions, respectively. The ^{31}P MRS parameters were sampling points 1024, spectral width 4 kHz, slice thickness of 2.0 cm, slice number 10, TR 2 sec, and NA 32. The scan time was 22 mins, and this experiment was conducted on two subjects.

Single slice 2D multi-voxel MR spectra were acquired with in-plane (AP-RL) resolution of 1.0 × 1.0 cm^2, data matrix 16 × 15, sampling points 1024, spectral width 4 kHz, TR 2 sec and NA 4. The scan time was 32 min, and this experiment was conducted on two subjects.

^{31}P Spectral Analysis

The time-domain ^{31}P data were zero-filled to 8 k (for non-localized MRS) or 2 k (for 1D and 2D MRS), and applied by a line-broadening factor of 6 Hz (for non-localized MRS) or 9 Hz (for 1D and 2D MRS) prior to Fourier transformation. The frequency-domain ^{31}P spectra were phased and baseline corrected, and each of the sharp metabolite signals (including PE, PC, GPE, Pi^{ex}, Pi^{in}, GPC, PCr, NAD/NADH, α-, β- and γ-ATP) was fitted by a Voigt lineshape (a combination of Gaussian and Lorentzian lineshape) using ACD software (Advanced Chemistry Development, Inc., Toronto, Canada). For the residual phospholipid signals (broad baseline "bumps" with a long tail) embedded at the base of sharp phosphoester signals, a two-component Voigt lineshape was used for the fitting. To reduce potential fitting error on the small Pi^{ex} signal with OVS-on, a regional fitting (4.5 – 5.5 ppm) was performed with Pi^{ex} linewidth constricted to no less than half and no more than twice that of Pi^{in}. No constriction or prior knowledge was applied to the fitting of the remaining large ^{31}P signals. The intracellular concentration was evaluated using the γ-ATP signal as an internal concentration reference ($[ATP]_{in}$ = 3 mM) as described before (1, 2).

The intra- and extra-cellular pH values were obtained from the chemical shifts of the corresponding P_i peaks (δ_{Pi}, in ppm) referenced to PCr (δ = 0 ppm) using the following formula:

$$pH = pKa + \log\frac{\delta_{Pi} - \delta_a}{\delta_b - \delta_{Pi}} \quad [1]$$

A $H_2PO_4^- \leftrightarrow H^+ + HPO_4^{2-}$ acid dissociation constant, *pKa*, of 6.73 along with ^{31}P limiting shifts δ_a = 3.275 ppm (for acidic protonated species $H_2PO_4^-$) and δ_b = 5.685 ppm (for basic deprotonated species HPO_4^{2-}) were used to calculate the pH values.

Estimate of Pi in interstitial fluid

Assuming that the volume of the cerebral tissue is composed of extracellular and intracellular spaces with a volume fraction of α and (1 - α), respectively, then the relative signal intensity of extra- and intracellular Pi intensity is governed by

$$\rho = \beta \bullet \alpha/(1-\alpha) \quad [2]$$

where β denotes the ratio of extra- to intra-cellular Pi concentration (= $[Pi]_{ex}/[Pi]_{in}$), and ρ denotes the ratio of Pi^{ex} to Pi^{in} signal intensity. Assuming the extracellular space is occupied solely by the interstitial fluid (ISF), then one can estimate the ISF Pi concentration by

$$[Pi]_{ISF} = \rho \bullet (1-\alpha)/\alpha \bullet [Pi]_{in} \quad [3]$$

Statistical Analysis

All data are reported as mean ± standard deviation, calculated using Matlab. The difference between two sets of data are considered to be statistically significant when *p*-value <= 0.05.

RESULTS

Outer-volume suppression (OVS)

Figure 1 shows two 7T ^{31}P MR spectra, one with and another without OVS saturation (red versus blue trace), collected from the same posterior region of human brain at resting state. The OVS was generated by four ^{31}P saturation slabs placed over the meningeal tissue close to the coil surface (Figure 1a, for clarity, only three OVS slabs are shown). The unintended OVS spillover effect (18 ± 5 %, N = 7) on the brain tissues was corrected by scaling both spectra to PCr as reference, which is the most abundant P-metabolite in the brain but virtually absent in the blood and CSF. As highlighted in Figure 1b, OVS saturation resulted in attenuation of the signal associated with extracellular inorganic phosphate (P_i^{ex}). This P_i^{ex} attenuation effect was observed in all seven subjects studied by OVS; the average P_i^{ex} signal attenuation (ΔS/S) was 67 ± 9% (Figure 2a, *p*-value = 0.01, N = 7). From the measured P_i^{ex} /P_i^{in} ratio in the OVS attenuated spectra, the extracellular P_i concentration was estimated at 0.51 ± 0.07 mM, assuming an extracellular volume fraction of 20% (16, 17).

In addition to attenuating Pi^{ex} signal intensity, OVS saturation also led to a slight yet statistically significant upfield shift in the remaining Pi^{ex} signal ($\Delta\delta$ = 0.06 ± 0.02, Figure 1c), equivalent to a pH change (ΔpH) of 0.07 unit, from pH 7.39 ± 0.04 without OVS to pH 7.32 ± 0.03 with OVS saturation (Figure 2b, *p*-value = 0.03, N = 7).

In addition to P_i^{ex} (Figure 1b), a ^{31}P signal co-resonating with phosphoethylamine (PE) was also attenuated by OVS saturation. The spectral subtraction (off – on) showed that the attenuated peak has an asymmetric lineshape with a broad tail on the downfield side of the peak (Figure 1b). For the group of the subjects studied by OVS (N = 7), the average attenuation for this signal upon OVS saturation was 40 ± 7%.

1D Multi-slice ^{31}P MRS

To investigate the basis of these OVS saturation observations, additional 1D CSI ^{31}P MR spectra were collected from multiple slices in the brain along the anatomical direction of either head-to-feet (HF, Figure 3) or anterior-to-posterior (AP, Figure 4). Depending upon the anatomical locations, these brain slices differ in the meningeal volume fraction (consequently blood volume fraction) so might be expected to yield different ^{31}P spectral patterns in the downfield region from Pi to phosphomonoesters (PME) (see discussion later).

As shown in Figures 3 and 4, irrespective of the slice orientation, larger Pi^{ex}/ Pi^{in} and PME/ Pi^{in} signal ratios, together with a wider inter-peak gap (Δδ) between Pi^{ex} and Pi^{in} signals, and a higher raised spectral baseline in the Pi^{ex} and downfield region, were observed for the slices with larger meningeal volume fractions. For example, in the multi-slice brain ^{31}P spectra acquired along the AP direction (Figure 4), the signal intensity of the Pi^{ex} in reference to Pi^{in} is increased by approximately fivefold from top to bottom slices. In parallel,

the center resonance frequency of the Pi^{ex} peak is shifted downfield, from 5.22 ppm to 5.30 ppm, corresponding to a media alkalization of 0.10 pH unit (from pH 7.35 to pH 7.45), while the Pi^{in} peak showed only a minor downfield shift, from 4.79 ppm to 4.82 ppm, corresponding to an intracellular pH change of 0.02 unit (from pH 7.96 to pH 7.98).

2D Multi-voxel ^{31}P MRS

To further validate the findings by non-localized OVS and 1D multi-slice ^{31}P MRS, we acquired multi-voxel 2D CSI ^{31}P MR spectra in the posterior region of the brain (Figure 5), which permits regrouping of the spectral data from selected voxels in regions with similar anatomical features. To compare the ^{31}P spectral difference between different anatomical regions, two summed spectra were generated from the multi-voxel dataset, each by combining the data from twelve voxels (Figure 5a), one from the peripheral region with a high meningeal volume fraction (Figure 5a, red trace), and another from the deeper cerebral region with a high parenchymal volume fraction (containing mainly neurons and glial cells) (Figure 5a, blue trace).

As compared in Figure 5a, when scaled to PCr, the summed ^{31}P spectrum acquired from the peripheral region (red trace) yielded a Pi^{ex} signal 4.5 fold larger than that from the deeper cerebral parenchymal region (blue trace), while there was virtually no difference in Pi^{in} signal intensity. As for Pi^{ex} chemical shift, the meningeal region was shifted 0.13 ppm downfield from the inner cerebral region (5.37 ppm versus 5.24 ppm, Figure 5a, the highlighted region). In contrast, the difference in Pi^{in} signal was negligible between these two regions (meningeal 4.82 ppm versus cerebral 4.83 ppm).

As in the Pi^{ex} region, similar signal differences were also detected in the downfield PME region, where the summed spectrum from the peripheral voxels yielded broader and larger signals compared to those from the deeper cerebral voxels (Figure 5a).

DISCUSSION

Sources of “hidden” Pi component

Supported by the localized 1D (“multi-slice”) and 2D (“multi-voxel”) ^{31}P MRS data (Figures 3–5), we have demonstrated the presence of a previously unrecognized “hidden” Pi component, which accounts for about 2/3 of the total Pi^{ex} signal, in the fully-relaxed brain ^{31}P MR spectrum acquired by a non-localized pulse sequence (Figure 1). These combined observations suggest that the “hidden” component in the Pi^{ex} signal originates from the peripheral region of the brain, which can be effectively attenuated by OVS saturation (Figure 1).

The phenomenon of the Pi^{ex} signal attenuation by OVS cannot be simply a result of spectral artefact, given the consistency of the observation among all subjects and of the findings by different detection methods (Figures 1, 3–5). Is the phenomenon caused by MT effect? The short duration of the OVS pulse (1.8 ms) and a lack of post-OVS delay may argue against any significant MT effect that might exist between Pi^{ex} and broad baseline signals of phospholipids. In fact, a previous off-resonance saturation (ORS) study by McNamara (18) showed that, even with a long-duration pulse two order of magnitude longer than the OVS

pulse used here, no obvious signal reduction occurs at the alkaline Pi component (Pi^{ex}) in the human head, while the broad baseline signal from phospholipids and the bones of the skull was effectively diminished through MT effect. This implies that there is a lack of MT effect between Pi^{ex} and broad baseline signals of phospholipids. Furthermore, ample data are available in literatures (1–4) to support the view that the Pi^{ex} represents a metabolically inert pool; no measureable phosphoryl exchange MT effect occurs at Pi^{ex} when the ATP and PCr resonances are saturated or inverted (1–4). Together all these data confirm that direct saturation of an outer-volume component rather than MT effect is likely the predominant mechanism responsible for the phenomenon of the Pi^{ex} signal attenuation by OVS. We tentatively assign the primary source of the attenuated Pi^{ex} component to blood serum Pi for the following reasons:

1. the presence of a sizable pool of blood flowing in the intravascular spaces embedded in the meningeal tissues (Figure 1a, 3b and 4b) are in the high sensitivity region of the ^{31}P surface coil used for detection;
2. the presence of a high concentration of Pi in normal blood serum (1.29 ± 0.17 mM (19), versus 0.85 ± 0.17 mM for Pi in the intracellular space (1));
3. a higher media pH in the blood than in the ISF (7.35 – 7.45 versus 7.24 ± 0.07 (20)), which is compatible to the observation of an upfield change in the Pi^{ex} signal upon OVS saturation (corresponding to a pH lowering from 7.39 ± 0.03 to 7.32 ± 0.04) ; and
4. the consistency between the extracellular Pi concentration 0.51 ± 0.07 mM (estimated from the Pi^{ex} intensity measured with OVS on) and the documented extracellular Pi levels in the ISF (0.61 mM (21), 0.5 – 1.0 mM (15)).

A secondary source for this “hidden” Pi component might be the CSF. The Pi level of the CSF is about one-half of that of blood serum (22). While ventricular CSF is relatively far from the most sensitive region of the surface coil, there is a small pool of CSF present in the fibrous subarachnoid space within the meninges which is close to the RF coil. If visible by the ^{31}P detection, its contribution to the Pi^{ex} signal is expected to be on the upfield side, as the CSF is less alkaline than the blood serum (CSF pH 7.33 versus blood serum pH 7.41 (23)). However, the Pi^{ex} signal attenuation induced by OVS of occurs on the downfield side, which argues against CSF as a significant contributor to the observed Pi^{ex} signal.

Together with the observation of a 67% reduction in Pi^{ex} signal area upon OVS saturation of meningeal tissues, another closely related finding is a concurrent 40% signal reduction in the region of PME co-resonating with PE (Figure 1b). Indeed, the PME signals appear to be much larger in the peripheral meningeal region than in the deeper cerebral region, as clearly revealed by localized 1D and 2D MRS data (Figures 3c, 4c and 5a). The phenomenon could be explained if high levels of PME are present in cortical tissues included in the selected slices and voxels due to partial volume effects. However, this appears to be in conflict with the finding of a previous localized ^{31}P MRS study that reported a lower level of PME in the cortical grey matter than in the deeper cerebral tissues (24). Since the lineshape of the OVS-attenuated signal at PE (Figure 1b, subtraction trace) appeared to be asymmetric with features similar to a typical membrane phospholipid signal due to chemical shift anisotropy

(CSA) effect (25), this signal could be attributed to a mobile membrane phospholipid component, which might be decayed out in the early localized ^{31}P study (24).. Another possible explanation is that the mobile membrane phospholipid component that co-resonates with PE was contributed from the outer-volume tissues (such as meninges and scalp tissues).

An alternative source of the extra ^{31}P signal under PME may be the blood 2,3-diphosphoglycerate (DPG), a metabolite abundantly present in the red blood cells with a typical RBC concentration of ~ 5.3 mM (26), which is about 5-fold more abundant than Pi in normal blood serum. Though its chemical shifts depend on blood oxygenation (27), RBC 2,3-DPG has been reported to be 100% visible in vitro by ^{31}P NMR. Observation of blood 2,3-DPG ^{31}P signals have been reported in the PME and Pi region (5 – 7 ppm) in several cardiac ^{31}P studies in vivo (28–33). In some cases, the 2,3-DPG signals can be resolved into two separate peaks (29, 33). However, a characteristic doublet resonance pattern was not present in our brain ^{31}P spectra. This might be due to the blood pool size being small in brain posterior region as compared to in a typical heart. It may also be caused by line broadening and/or chemical shift dispersion due to variation in blood flow and oxygenation, and magnetic susceptibility anisotropy (MSA) of blood vessels/sinuses and the enclosing layer-structured meningeal tissues. Taken together, further studies are needed to evaluate whether blood 2,3-DPG or mobile membrane phospholipids or something else is the correct assignment to the OVS-attenuated signal at the resonance frequency of PE.

It should be pointed out that, though major broad signals of the membrane phospholipids and the bones of the skull, which typical accounts for 80% of total brain phosphate signals with a linewidth in the order of 1 kHz (18), was filtered out in our study by setting the acquisition sequence DT to 0.5 ms, the residual narrower signals from motion less-restricted macromolecules or mobile phospholipids could filter through and showed as small broad “bumps” at the base of the sharp phosphoester signals (Figures 1, 3–5). These signals are featured with a long tail which may reflect the chemical shift anisotropy (CSA). Also, it should be noted that, due to the natural curvature of human skull, there was an inevitable partial volume effect in human brain ^{31}P spectra when the OVS slabs were applied on the outer-volume tissues (meninges, skull and scalp). This led to a considerable reduction of brain MRS signals (18 ± 5%, N =7) as spillover side effect.

Potential implications

Despite the increasing trend of using localized technique with volume coil, conventional pulse-acquire sequence together with a surface coil is still the most practical or easiest way to measure low abundant P-metabolites (34–37). The multi-component nature of the brain P_i^{ex} signal as revealed by our ^{31}P MRS data illustrates that one must be cautious when interpreting non-localized spectra for measuring energy metabolism and tissue pH. This is especially true at lower magnetic fields since the individual Pi components detected here at 7T are technically difficult to detect at lower fields. Fortunately, with ^{31}P OVS method becoming increasingly available in high field scanners, it can be used to obtain a true measure of intra- and extracellular Pi effectively eliminating contaminating ^{31}P signals from blood. Contamination of PME signals may also have implications in studies of phospholipid

metabolites using ^{31}P MRS since PME/PDE ratio is an indicator of altered phospholipid metabolism in aging and cancer (38, 39).

Perhaps equally importantly, the visibility of meningeal blood Pi signal may offer new opportunities for brain injury studies using ^{31}P MRS. One might expect to see an increased Pi signal if blood accumulates in the meninges as result of head injury. Two potential spaces for blood build-up include the epidural space between the dura and the skull (typically it occurs in young adults, and males are more often affected than females (40)), and the subdural space between the dura mater and the arachnoid mater (chronic subdural hematomas are common in the elderly (41)).

Once the extracellular Pi signal is cleared of contamination by OVS or localized ^{31}P MRS, it can be reliably used for measuring extracellular pH and Pi concentration. Such measurements established for normal healthy subjects could be useful for monitoring extracellular environmental changes under abnormal conditions, given that the extracellular space acts as a buffer to absorb the H^+ ions released from energetically compromised cells and to cope with cell volume changes caused by cerebral edema following brain trauma or from nontraumatic causes such as ischemic stroke, cancer or brain inflammation (42, 43).

In conclusion, We have demonstrate the presence of a phosphate signal co-resonating with extracellular inorganic phosphate in brain ^{31}P spectra acquired by non-localized MRS. The most likely source for this previously unrecognized phosphate signal is peripheral meningeal fluids, especially the venous blood. Mobile phospholipids and/or blood 2,3-DPG may also interfere the PME signal and the spectral baseline in the downfield region. These observations have implications in using the Pi^{ex} signal as an endogenous probe of tissue pH and using the PME signal as a biomarker of phospholipid metabolism. When Pi^{ex} and Pi^{in} cannot be resolved for example at low magnetic fields or in tissues of high heterogeneity, without taking into account of blood serum Pi contribution to the total Pi signal may lead to data misinterpretation. On the other hand, there may be new opportunities to use ^{31}P MRS for studies of abnormal Pi levels due to alteration in CSF or blood volume change in cases such as head injury.

Acknowledgments

The authors are grateful to Ivan Dimitrov (Philips Healthcare) for technical support and Salvador Pena for operational assistance. Jeannie Baxter and Janet Jerrow recruited and managed the human subjects. This project was supported by the National Center for Research Resources and the National Institute of Biomedical Imaging and Bioengineering of the National Institutes of Health through P41EB015908, DK081186, R37-HL-034557, P01DK058398 and RO1AR050597, Department of Defense Grant W81XWH-06-2-0046.

References

1. Ren J, Sherry AD, Malloy CR. Efficient ^{31}P band inversion transfer approach for measuring creatine kinase activity, ATP synthesis, and molecular dynamics in the human brain at 7T. Magn Reson Med. 2016 Nov 20.doi: 10.1002/mrm.26560
2. Ren J, Sherry AD, Malloy CR. ^{31}P-MRS of healthy human brain: ATP synthesis, metabolic concentration, pH and T_1 relaxation times. NMR Biomed. 2015; 28(11):1455–62. [PubMed: 26404723]

3. DU F, Zhu XH, Qiao H, Zhang X, Chen W. Efficient in vivo ^{31}P magnetic transfer approach for noninvasively determining multiple kinetic parameters and metabolic fluxes of ATP metabolism in the human brain. Magn Reson Med. 2007; 57(1):103–14. [PubMed: 17191226]
4. Tiret B, Brouillet E, Vallette J. Evidence for a “metabolic inactive” inorganic phosphate pool in adenosine triphosphate synthase reaction using localized ^{31}P saturation transfer magnetic resonance spectroscopy in the rat brain at 11.7T. J Cereb Blood Flow Metab. 2016; 36(9):1513–8. [PubMed: 27354096]
5. Kintner DB, Anderson MK, Sailor KA, Dienel G, Fitzpatrick JH Jr, Gillboe DD. In vivo microdialysis of 2-deoxyglucose 6-phosphate into brain: a novel method for the measurement of interstitial pH using ^{31}P-MR. J Neuochem. 1999; 72(1):405–12.
6. Bobko AA, Eubank TD, Driesschaert B, Dhimitruka I, Evans J, Mohammad R, Tchekneva EE, Dikov NM, Khramtsov VV. Interstitial inorganic phosphate as a tumor microenvironment marker for tumor progression. Sci Rep. 2017; 7:41233. [PubMed: 28117423]
7. Chesler M. Regulation and modulation of pH in the brain. Physiol Rev. 2003; 83(4):1183–221. [PubMed: 14506304]
8. Chen ZL, Huang RQ. Extracellular pH modulate GABAergic neurotransmission in rat hypothalamus. Neuroscience. 2014; 271:64–76. [PubMed: 24780768]
9. Gerweck LE, Seetharaman K. Cellular pH gradient in tumor versus normal tissue: potential exploitation for treatment of cancer. Cancer Res. 1996; 56(6):1194–8. [PubMed: 8640796]
10. Dirmagl U. Pathobiology of injury after stroke: the neurovascular unit and beyond. Ann N Y Acad Sci. 2012; 1268:21–5. [PubMed: 22994217]
11. Aibiki M, Kawaguchi S, Maekawa N. Reversible hypophosphatemia during moderate hypothermia therapy for brain-injured patiens. Crit Care Med. 2001; 29:1726–30. [PubMed: 11546972]
12. Larsen BR, MacAulay N. Activity-dependent astrocyte swelling is mediated by pH-regulating mechanisms. Glia. 2017 Jul 26.doi: 10.1002/glia.23187
13. Timofeev I, Nortje, Al-Rawi PG, Hutchinson PJ, Gupta AK. Extracellular brain pH with or without hypoxia is a marker of profound metabolic derangement and increased mortality after traumatic brain injury. J Cereb Blood Flow Metab. 2013; 33(3):422–7. [PubMed: 23232949]
14. Mohseni M, Chiota N, Roy A, et al. Severe hypophosphatemia and acute neurologic dysfunction in a marathon runner. Clin J Sport Med. 2011; 21:269–70. [PubMed: 21422917]
15. Dallaire L, Beliveau R. Phosphate transport by capillaries of the blood-brain barrier. J Biol Chem. 1992; 267(31):22323–7. [PubMed: 1429584]
16. Madelin G, Kline R, Walvick R, Regatte RR. A method for estimating intracellular sodium concentration and extracellular volume fraction in brain in vivo using sodium magnetic resonance imaging. Sci Rep. 2013; 4:4763.
17. Hrabetova S, Nicholson C. Biophysical properties of brain extracellular space explored with ion-selective microelectrode, integrative optical imaging and related techniques. In: Michael AC, Borland LB, editorsElectrochemical Methods for Neuroscience. CRC Press/Taylor & Francis; Boca Raton: 2007. (Free Access Online: www.crcnetbase.com/isbn/978-0-8493-4075-8)
18. McNamara R, Arias-Mendoza F, Brown TR. Investigation of broad resonances in ^{31}P NMR spectra of the human brain in vivo. NMR Biomed. 1994; 7:237–242. [PubMed: 7848814]
19. Bansal VK. Serum Inorganic Phosphorous. In: Walker HK, Hall WD, Hurst JW, editorsClinical Method: The History, Physical, and Laboratory Examinations. 3. Boston: Butterworth; 1990.
20. Nedergaard M, Kraig RP, Tanabe J, Pulsinelli WA. Dynamics of interstitial and intracellular pH in evolving brain infarct. Am J Physiol. 1991; 260:R581–588. [PubMed: 2001008]
21. Fogh-Anderen N, Altura BM, Altura BT, Siggaard-Andersen O. Composition of interstitial fluid. Clin Chem. 1995; 41(1):1522–25. [PubMed: 7586528]
22. Guerreiro PM, Bataille AM, Parker SL, Renfro JL. Active removal of inorganic phosphate from cerebral fluid by the choroid plexus. Am J Physiol Renal Physiol. 2014; 306:F1275–F1284. [PubMed: 24740787]
23. Irani DN. Cerebrospinal Fluid in Clinical Practice. Philadelphia: Saunders; 2009. 311
24. Buchli R, Duc CO, Martin E, Boesiger P. Assessment of absolute metabolite concentrations in human tissue by ^{31}P MRS in vivo. Part I: cerebrum, cerebellum, cerebral gray and white matter. Magn Reson Med. 1994; 32:447–52. [PubMed: 7997108]

25. Mani R, Cady SD, Tang M, Waring AJ, Lehrer RI, Hong M. Membrane-dependent oligomeric structure and pore formation of a beta-hairpin antimicrobial peptide in lipid bilayers from solid-state NMR. Proc Natl Acad Sci U S A. 2006; 103(44):16242–7. [PubMed: 17060626]
26. Gupta RK, Benovic JL, Rose ZB. the determination of the free magnesium level in the human red blood cell by ^{31}P NMR. J Bio Chem. 1978; 253(17):6172–76. [PubMed: 687387]
27. Bashir A, Bohnert KL, Reeds DN, Peterson LR, Bittel AJ, de las Fuentes L, Pacak CA, Byrne BJ, Cade WT. Impaired cardiac and skeletal muscle bioenergetics in children, adolescents, and young adults with Barth syndrome. Physiol Rep. 2017; 5(3):e13130. [PubMed: 28196853]
28. Schmidt O, Bunse M, Dietze GJ, Lutz O, Jung W. Unveiling extracellular inorganic phosphate signals from blood in human cardiac ^{31}P NMR spectra. J Cardiovasc Magn Reson. 2001; 3(4): 325–9. [PubMed: 11777224]
29. Petersen A, Kristensen SR, Jacobsen JP, Horder M. ^{31}P-NMR measurements of ATP, ADP, 2,3-diphosphoglycerate and Mg2+ in human erythrocytes. Biochim Biophys Acta. 1990; 1035:169–74. [PubMed: 2393665]
30. Zhang J, Ugurbil K, From AH, Bache R. Myocardial oxygenation and high energy phosphate levels during graded coronary hypoperfusion. Am J Physio – Heart and Circulatory Physilogy. 2001; 280(1):H318–H326.
31. Jones DE, Hollingsworth K, Fattakhova G, MacGowen G, Taylor R, Blamire A, Newton JL. Impaired cardiovascular function in primary biliary cirrhosis. Am J Physiol. – Gastrointest Liver Physiol. 2010; 298:G764–G773. [PubMed: 20133949]
32. Xiong Q, Zhang P, Guo J, Swingen C, Jang A, Zhang J. Myocardial ATP hydrolysis rates in vivo: a porcine model of pressure overload-induced hypertrophy. Am J Physiol – Heart and Circulatory Physilogy. 2015; 309(3):H450–H458.
33. Jung WI, Sieverding L, Breuer J, Hoess T, Widmaier S, Schmidt O, Bunse M, Erckelens F. ^{31}P NMR spectroscopy detects metabolic abnormalities in asymptomatic patients with hypertrophic cardiomyopathy. Circulation. 1998; 97:2536–42. [PubMed: 9657474]
34. De Graaf RA, De Feyter HM, Brown PB, Nixon TW, Rothman DL, Behar KL. Detection of cerebral NAD+ in humans at 7T. Magn Reson Med. 2017; 78(3):828–35. [PubMed: 27670385]
35. Du F, Yuksel C, Chouinard VA, Huynh P, Ryan K, Cohen BM, Ongur D. Abnormalities in high-energy phosphate metabolism in first-episode bipolar disorder measured using ^{31}P magnetic resonance spectroscopy. Biol Psychiatry. 2017 S0006-3223(17):31466-x.
36. Nelander M, Weis J, Bergman L, Larsson A, Wikstrom AK, Wikstrom J. Cerebral magnesium levels in preeclampia; a phosphrous magnetic resonance spectroscopy study. Am J Hypertens. 2017; 30(7):667–72. [PubMed: 28338765]
37. Bonvento G, Valette J, Flament J, Mochel F, Brouillet E. Imaging and spectroscopic approaches to probe brain energy metabolism dysregulation in neurodegenerative diseases. J Cereb Blood Flow Metab. 2017; 37(6):1927–43. [PubMed: 28276944]
38. Wijnen JP, Scheenen TW, Klomp DW, Heerschap A. 31P magnetic resonance spectroscopic imaging with polarisation transfer of phosphomono- and diesters at 3 T in the human brain: relation with age and spatial differences. NMR Biomed. 2010 Oct; 23(8):968–76. [PubMed: 20669234]
39. Wijnen JP, Jiang L, Greenwood TR, van der Kemp WJ, Klomp DW, Glunde K. 1H/31P polarization transfer at 9.4 Tesla for improved specificity of detecting phosphomonoesters and phosphodiesters in breast tumor models. PLoS One. 2014 Jul 18.9(7):e102256. [PubMed: 25036036]
40. Ferri FF. Ferri's Clinical Advisor 2017 E-Book: 5 Books in 1. Elsevier Health Sciences. 2016:441.
41. Kushner D. Mild Traumatic Brain Injury: Toward Understanding Manifestations and Treatment. Archives of Internal Medicine. 1998; 158(15):1617–1624. [PubMed: 9701095]
42. Azzarito T, Lugini L, Spugnini EP, Canese R, Gugliotta A, Fidanza S, Fais S. Effect of Modified Alkaline Supplementation on Syngenic Melanoma Growth in CB57/BL Mice. PLoS One. 2016; 11(7):e0159763. [PubMed: 27447181]
43. Cea G, Bendahan D, Manners D, Hilton-Jones D, Lodi R, Styles P, Taylor DJ. Reduced oxidative phosphorylation and proton efflux suggest reduced capillary blood supply in skeletal muscle of

patients with dermatomyositis and polymyositis: a quantitative 31P-magnetic resonance spectroscopy and MRI study. Brain. 2002; 125(Pt 7):1635–45. [PubMed: 12077012]

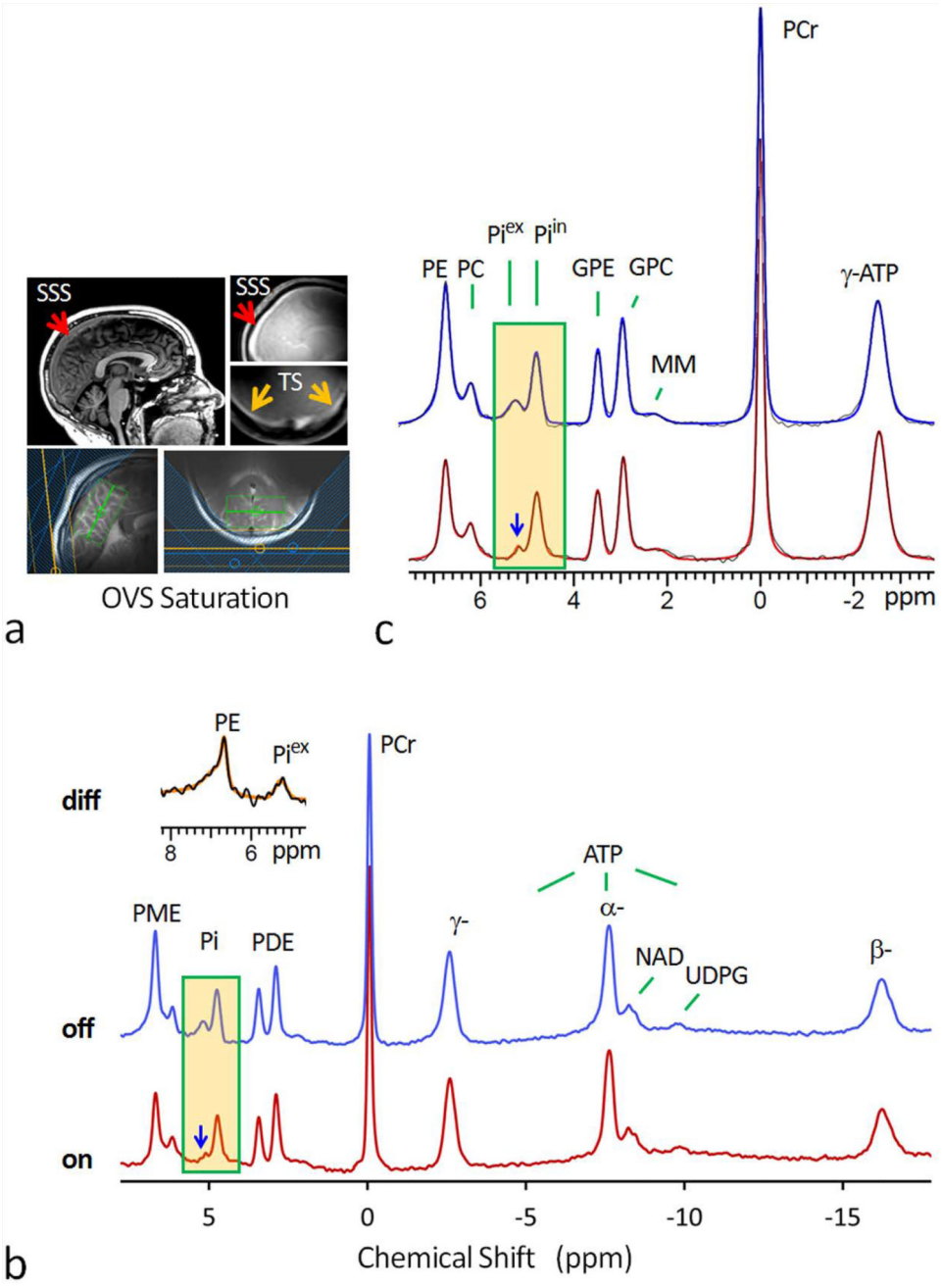

FIG. 1.

(a) 7T MR head images showing the location of superior sagittal sinus (SSS), transverse sinus (TS), and the ^{31}P saturation slabs for outer-volume-suppression (OVS). The green box in the images represents the ^{1}H shimming area. **(b)** Fully-relaxed 7T ^{31}P MR spectra at long TR of 30 sec, acquired from resting human brain using a pulse-acquire sequence with (red trace) and without (blue trace) OVS saturation. Note the marked attenuation of the signals at Pi^{ex} and PE upon OVS saturation, while other metabolite ^{31}P signals remain unchanged in reference to PCr at 0 ppm. Also note the asymmetric lineshape of the attenuated peak at PE (inset) as featured in typical membrane phospholipid signal due to chemical shift anisotropy

effect. **(c)** The fitted ^{31}P MR spectra in the chemical shift region between -4.0 and 8.0 ppm (red trace: OVS on; blue trace: OVS off). Abbreviation: PE, phosphoethenolamine; PC, phosphocholine, GPE, glycerophosphoethanolamine; GPC, glycerophosphocholine; Pi^{in} and Pi^{ex}, intra- and extracellular inorganic phosphate; PCr, phosphocreatine; ATP, adenosine triphosphate; NAD, nicotinamide adenine dinucleotide; UDPG, uridine diphosphate glucose; PME, phosphomonoester; PDE, phosphodiester; MM, macromolecules (likely from mobile membrane phospholipids).

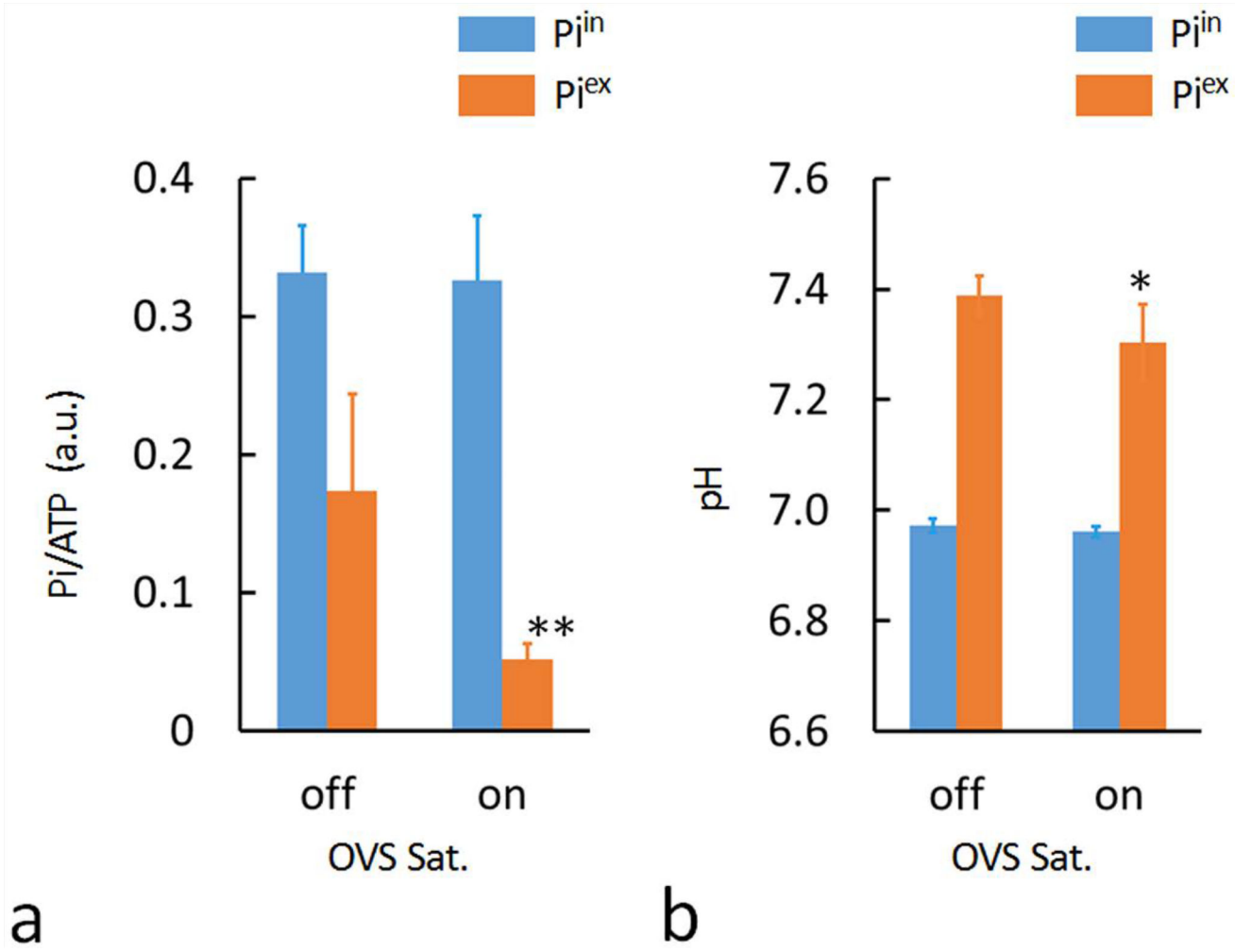

FIG. 2.

Plots of the brain Pi-to-γATP ratio **(a)** and pHs **(b)** with and without OVS saturation, measured for the group of subjects (N = 7 subjects). OVS saturation led to significant reduction in both extracellular pH (*p*-value = 0.03) and Pi signal intensity (*p*-value = 0.01).

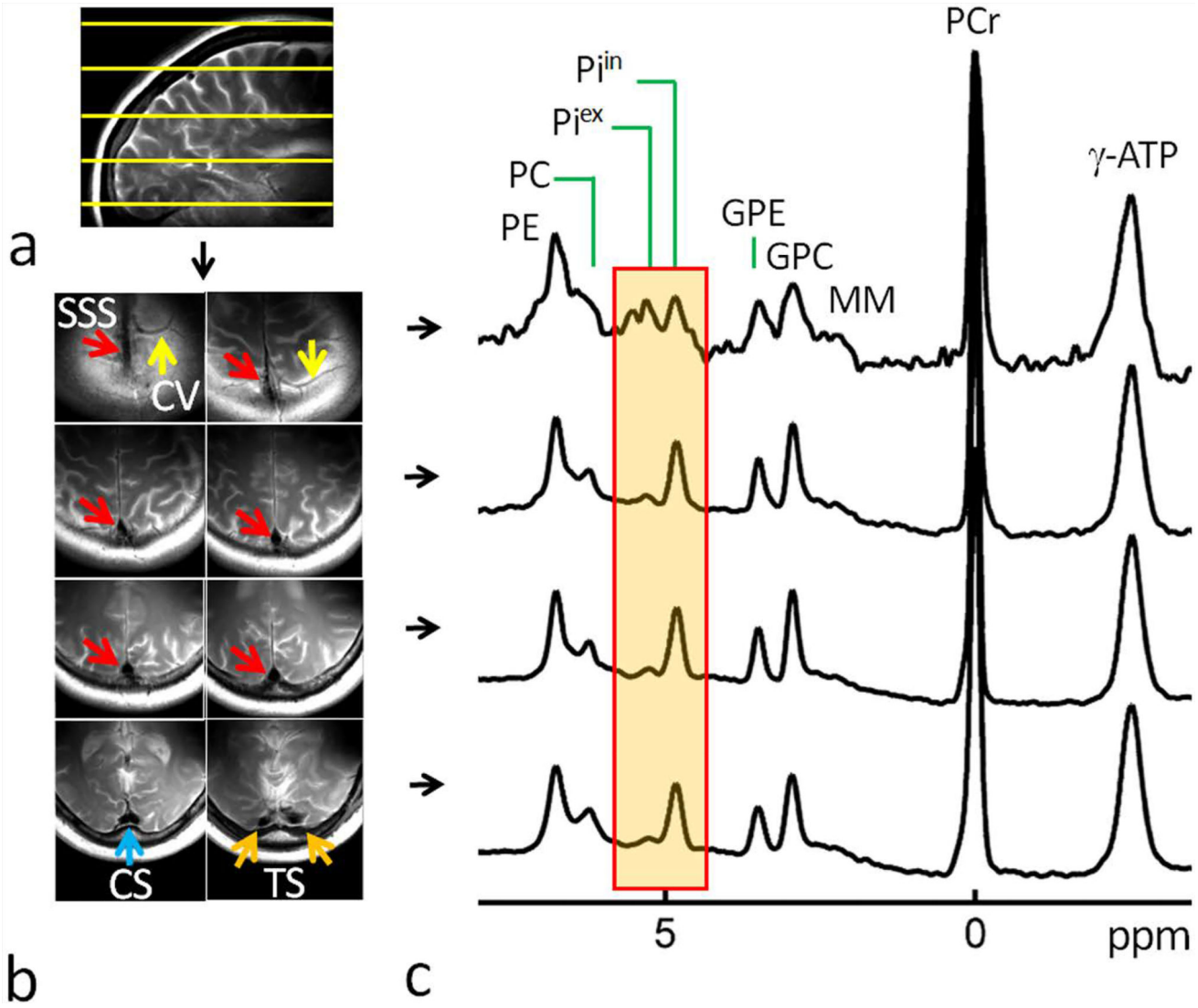

FIG. 3.

(a) A brain sagittal T2w Image showing the planning of multi-slice ^{31}P MRS w along HF direction (top to bottom). **(b)** Brain axial T2w Images acquired in the region of selected spectral slices with colored arrows indicating cerebral veins (CV, yellow), superior sagittal sinus (SSS, red), confluence of sinuses (CS, blue), and transverse sinus (TS, orange). **(c)** 1D multi-slice brain ^{31}P MR spectra acquired along HF direction (from top to bottom) at 7T with a short TR of 2 sec and without OVS saturation. Note the decreasing trend of the ratio Pi^{ex}-to-Pi^{in} from top to bottom slices. Abbreviation: PE, phosphoethenolamine; PC, phosphocholine, GPE, glycerophosphoethanolamine; GPC, glycerophosphocholine; Pi^{in} and Pi^{ex}, intra- and extracellular inorganic phosphate; MM, macromolecules (likely from mobile membrane phospholipids); PCr, phosphocreatine; ATP, adenosine triphosphate.

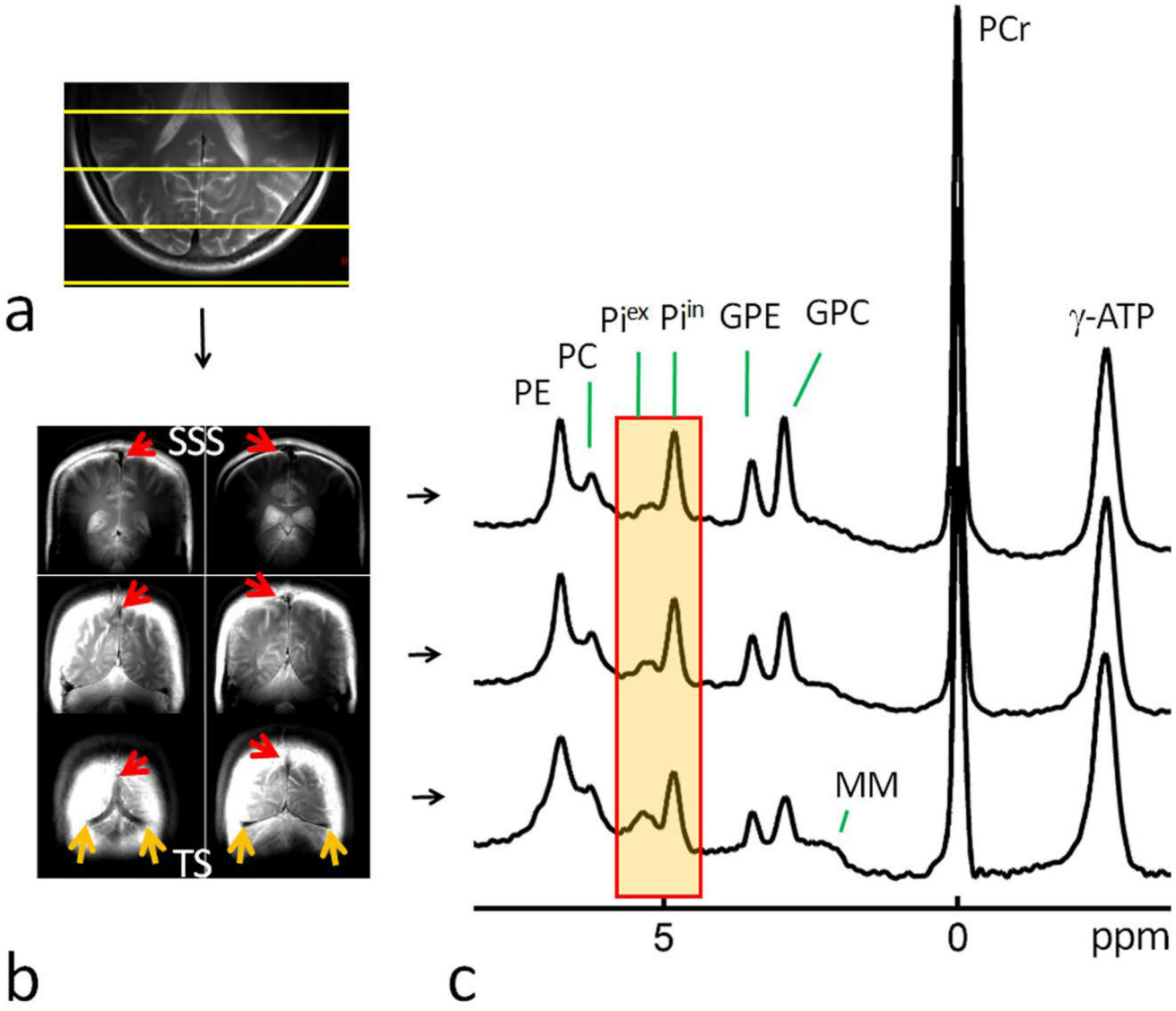

FIG. 4.

(a) A brain axial T2w image showing the planning of multi-slice ^{31}P MRS along AP direction (top to bottom). **(b)** Brain coronal T2w Images acquired in the region of selected spectral slices with colored arrows indicating superior sagittal sinus (SSS, red) and transverse sinus (TS, orange). **(c)** 1D multi-slice brain ^{31}P MR spectra acquired along AP direction (from top to bottom) at 7T with a short TR of 2 sec and without OVS saturation. Note the increasing trend of the ratio Pi^{ex}-to-Pi^{in} from top to bottom slices. Abbreviation: PE, phosphoethenolamine; PC, phosphocholine, GPE, glycerophosphoethanolamine; GPC, glycerophosphocholine; Pi^{in} and Pi^{ex}, intra- and extracellular inorganic phosphate; MM, macromolecules (likely from mobile membrane phospholipids); PCr, phosphocreatine; ATP, adenosine triphosphate.

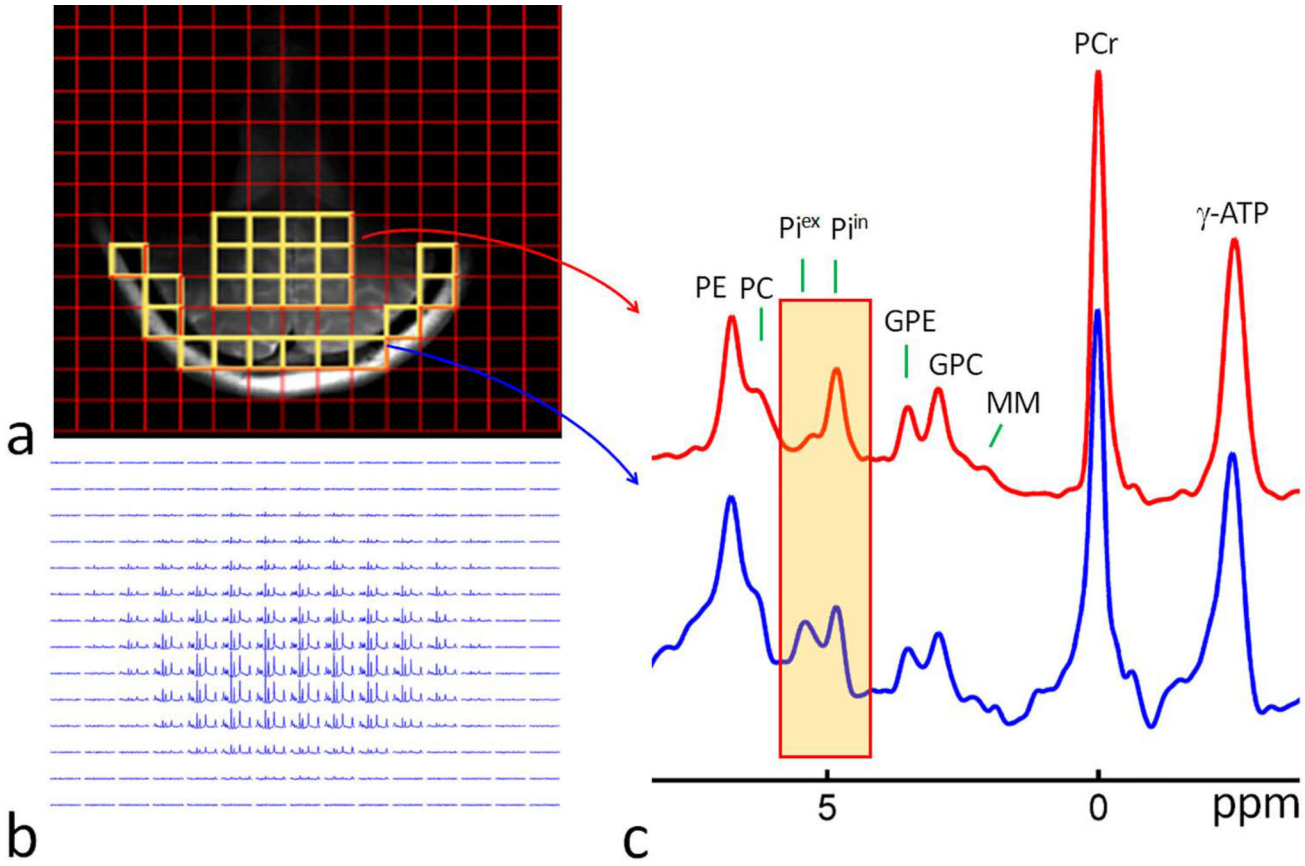

FIG. 5.

(a) Comparison of brain ^{31}P MR spectra between peripheral meningeal tissues (bottom, red trace) and deeper parenchymal tissues (top, blue trace), showing their difference in Pi^{ex} signal intensity and chemical shift. Both spectra were a sum of twelve selected voxels in selected region-of-interest (ROI) as illustrated in MR images on left panels (in yellow). **(b)** Brain 2D CSI ^{31}P MR spectral data matrix acquired with in-plane resolution of 10 × 10 mm^2 and TR 2 sec. Abbreviation: PE, phosphoethenolamine; PC, phosphocholine, GPE, glycerophosphoethanolamine; GPC, glycerophosphocholine; Pi^{in} and Pi^{ex}, intra- and extracellular inorganic phosphate; PCr, phosphocreatine; MM, macromolecules (likely from mobile membrane phospholipids); ATP, adenosine triphosphate.